Uncovering cortical layers with multi-exponential analysis: a region of interest study

Jakub Jamárik
Faculty of Medicine
Masaryk University
Brno, Czech Republic
461084@muni.cz

Lubomír Vojtíšek
Central European Institute of Technology
Masaryk University
Brno, Czech Republic
vojtisek@mail.muni.cz

Daniel Schwarz
Department of Simulation Medicine, Institute of Biostatistics and Analyses, Faculty of Medicine
Masaryk University
Brno, Czech Republic
schwarz@med.muni.cz

***Abstract*—Pathologies of the cerebral cortex often manifest at resolutions outside of the scope of conventional magnetic resonance imaging (MRI). Two different pathways aiming to overcome this limitation have emerged in recent years. One is focused on the direct imaging of the cortical layers achieved by increasing the MRI spatial resolution. The other approach relies on low-resolution images acquired at 3 T and represents the cortical layers in the domain of T_1 spin-lattice relaxation. In this work, we follow the T_1-mapping-based approach and explore two possible methods to achieve the representation of cortical layers: (1) modeling using a multi-exponential model, and (2) inverse Laplace transformation (ILT). Several regions of interest (ROI) across the cerebral cortex were measured and later used to create the ground-truth dataset. Using this data, the performance of the two models was evaluated. The ILT method proved superior to the multi-exponential model, yielding separation of all components with an average estimation error of 2.52 %. This method may enrich the low-resolution imaging framework by providing a more precise estimation of the spin-lattice spectrum.**

Keywords—cerebral cortex, exponential analysis, multi-exponential model, inverse Laplace transform, optimization, magnetic resonance imaging

I. Introduction

The separation of cortical layers *in vivo* is one of the major challenges in the field of neuroimaging. The laminar structure of the cerebral cortex carries vital information regarding the development and pathology of the brain. Malformations within the layers of the cortex can lead to several disorders. Due to the form of cortical layers, their sub-millimeter thickness, and uneven distribution within the cortex, their visualization using magnetic resonance imaging (MRI) still faces many obstacles. Several experimental works showed possible approaches in overcoming these limitations [1]–[6], resulting in the delineation of structures resembling cortical layers. These works used a multitude of methods, encompassing several MRI sequences such as magnetization-prepared fluid-attenuated inversion recovery sequence (FLAIR) [1], modified magnetization-prepared rapid acquisition gradient-echo (MPRAGE) sequence [2], [3], magnetization-prepared sequences of two rapid acquisition gradient-echoes (MP2RAGE) [4], and MP2RAGE in combination with multi-echo gradient-recalled echo (ME-GRE) sequence [5], [6]. This was facilitated in all cases by the usage of MRI at very high field strengths of 7 T. While leading to higher spatial resolutions, the highest field strengths also present different challenges of their own, such as larger distortions caused by the magnetic susceptibility artifact [7].

An alternative approach, using images with a lower resolution, has also emerged in the relevant literature [8]–[10]. This method relies on the acquisition of multiple images at lower resolutions and lower field strengths of 3 T. The cortical layers are then reconstructed from the images in the domain of T_1 spin-lattice relaxation. The delineation of cortical layers, made possible with this MRI sequence, is based on the differences in their myelination, which is reflected in their respective T_1 relaxation. Estimation of these relaxation parameters is achieved via mathematical modeling of intra-voxel cortical composition [9]. The resulting T_1 maps serve as the basis for the subsequent visualization pipeline, which projects the cortical layers onto the anatomical image using classification [10].

As stated previously, an important step of the low-resolution imaging approach is representing cortical layers in the spin-lattice domain. Given the form of the T_1 relaxation, this can be viewed as an exponential analysis problem. The exponential analysis is the numerical analysis of functions resulting from experimental measurements of phenomena exhibiting exponential decay [11]. The exponential function can be defined as:

$$f(t) = Ae^{-\frac{t}{\tau}} + B, \tag{1}$$

where A is the decay amplitude, B is the decay offset, and τ is the decay time constant. The goal of the exponential analysis is to estimate the amplitude and the time constant. If the measured data are assumed to originate from multiple exponentially decaying sources, the resulting signal can be viewed as a sum of exponential functions – each with a distinct time constant. The estimation of the parameters of these exponential functions is referred to as multi-exponential analysis.

In this work, we explore two possible methods of separating the cortical layers from low-resolution MRI images using multi-exponential analysis. These are the multi-exponential model and inverse Laplace transform (ILT). We assess the practicability of each method using datasets composed of different regions of interest (ROI), measured with an experimental low-resolution MRI sequence [9], and with ground-truth values of spin-lattice relaxation.

II. Materials and Methods

A. Data

Data were measured using a modified echo-planar imaging (EPI) sequence, with the following parameters: TR/TE = 1200/39 *ms*, 105 inversion times (*TI*) from the interval of 50 *ms* to 3000 *ms*, with the resolution of 3×3×3 mm^3. The size of the image obtained from this sequence was 64×64×42 voxels. The sequence was used to acquire a series of 105 images of four different anatomical ROIs. Three ROIs consisted of cortical gray matter (GM) and one of the cerebrospinal fluid (CSF). Voxels within the individual ROIs were averaged into four distinct ROI signals (see Fig. 1), representing the T_1 decay of the underlining tissue.

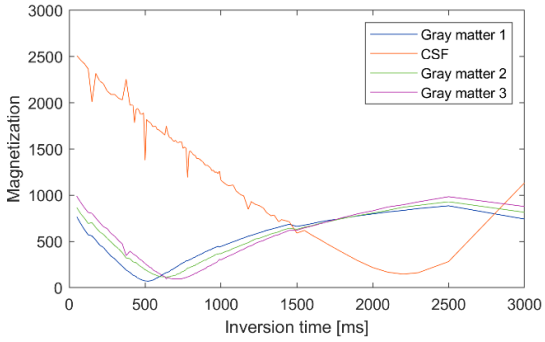

Fig. 1. The signal from measured regions of interest. The value of magnetization *M* (proportional ot the voxel intesity) changes depednig on the inversion time *TI*.

The last data point in each ROI was removed due to the loss of signal. Each of the ROI signals was fitted using a standard method for T_1 mapping [12] to estimate the mean T_1 relaxation time and mean magnetization M_0 within the signal. Following this, three combined signals were created by cumulatively adding the ROI signals together (see Fig. 2). This resulted in three datasets consisting of two, three, and four components, with ground-truth values of parameters T_1 and M_0.

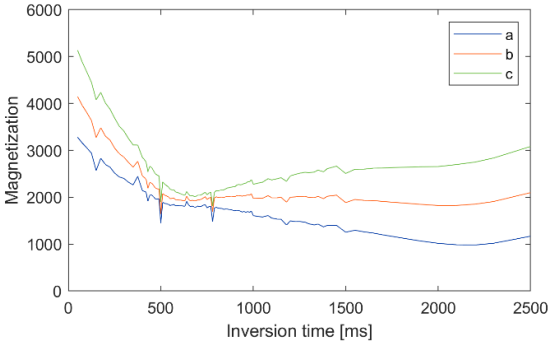

Fig. 2. The signal from combined regions of interest: a) two averaged components, b) three averaged components, c) four averaged components.

B. Multi-exponential modeling method

A multi-exponential model with a fixed number of components was used at first to separate the individual relaxation components:

$$M(TI_i) = \sum_{j=1}^{J} M_{0j}\,(1 - 2e^{-\frac{TI_i}{T_{1j}}}), \qquad (2)$$

where the magnetization for the *i*-th inversion recovery time $M(TI_i)$ is equal to the sum of individual magnetizations of the assumed components, M_{0j} is the magnetization at $TI = 0\ ms$ for the *j*-th component and T_{1j} is the T_1 relaxation time for the *j*-th component, and J denotes the number of components.

The model parameters are estimated by a nonlinear least-squares method. The least-square objective function is minimized using a modified trust-region algorithm. Trust-region algorithms approximate the objective function within an area of the search space, by finding a solution to the so-called trust-region sub-problem [13]. In each iteration, the algorithm builds a model of the objective function and optimizes it within the given trust-region. The trust-region is then modified based on the quality of the approximation provided by the model, increasing if sufficient and decreasing otherwise. We have modified this algorithm by repeatedly initializing the optimization procedure from multiple randomly chosen starting points [14]. Prior knowledge of the number of components within the composite signal was assumed.

C. Inverse Laplace transform method

The second method estimates the individual relaxation times using the inverse Laplace transformation. This term is used for a multitude of different methods [15]. In our work, we define the inverse Laplace transform as a solution to the Laplace integral equation, which in the context of our modeling approach takes the form:

$$M(TI) = \int_0^{\infty} g(T_1)(1 - 2e^{-\frac{\mathrm{TI}}{T_1}})dT_1, \qquad (3)$$

where $g(T_1)$ is a spectral function, representing the density of the distribution of all possible T_1 relaxation times. The solution $g(T_1)$ can be obtained by taking the inverse Laplace transform of (2). In practice, this is not feasible to achieve [11], instead (3) is linearized, giving:

$$M(TI_i) = \sum_j g(T_{1j})(1 - 2e^{-\frac{\mathrm{TI}_i}{T_{1\mathrm{j}}}}) + e_i, \qquad (4)$$

where $i \in \{1, \cdots, N\}$ is the number of measured inversion times, $j \in \{1, \cdots, J\}$ is the number of possible T_1 relaxation times and e_i is the experimental error. Equations (4) and (2) may seem similar, but they differ in the number of possible values of T_1 which can theoretically be estimated. In the case of (2), the number of possible T_1 values is equal to the number of assumed components, while in the case of (4), the number of possible T_1 values spans the interval of all candidate values for T_1. The solution to (4) is found using the following expression:

$$g = \arg min_{g \geq 0} \frac{1}{2} |A \cdot g - M|^2, \qquad (5)$$

where $A_{ij} = 1 - 2e^{-\frac{\mathrm{TI}_i}{T_{1\mathrm{j}}}}$ is the transformation kernel and $M = \left(M(TI_1), M(TI_2), \cdots M(TI_N)\right)$. Equation (5) is minimized using the nonnegative least squares algorithm [16].

III. Results

The resulting T_1 spectra obtained by the ILT are presented in Fig. 3.

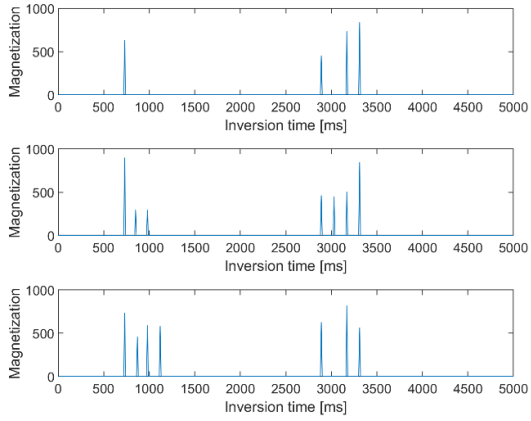

Fig. 3. T_1 spectra resulting from inverse Laplace transform.

Fig. 3 clearly demonstrates that the T_1 spectra contain more peaks than the individual components of combined ROIs. To compare the results with the ground truth, spectra were thresholded at the 60 % quantile and then iteratively binned. The number of bins was equal to the number of expected components. Each given peak was kept within its assigned component bin across all composite ROI if a similar peak manifested multiple times. The T_1 values in each bin were averaged, giving the final T_1 estimate for the given component. In case of the multi-exponential model, the estimates of M_0 and T_1 were output directly from the optimization routine. The resulting estimates of the parameters T_1 and M_0 are presented in Tables 1–3. Each table contains the absolute estimated values and relative errors achieved with the modified trust-region algorithm, ILT, and the ground-truth estimate.

TABLE I. Estimated coefficients for the two-component signal.

ID	Ground-truth		Modified trust-region algorithm		ILT
	T_1	M_0	T_1 abs/err[a]	M_0 abs/err	T_1 abs/err
CSF	728.90	910.02	910.02 / 0.31	907.17 / 1.05	730.00 / 0.15
GM1	3115.00	2605.50	2605.50 / 1.14	2576.10 / 2.98	3240.00 / 4.01

[a] abs-absolute value, err-relative error in %.

The multi-exponential model was able to distinguish all components that actually formed the combined ROI signal. The mean relative error of the T_1 estimates was 2.01 %, and the mean relative error of the M_0 was 0.73 %. The ILT method was able to distinguish all components with a mean T_1 relative error of 2.08 %.

TABLE II. Estimated coefficients for the three-omponent signal.

ID	Ground-truth		Modified trust-region algorithm		ILT
	T_1	M_0	T_1 abs/err[b]	M_0 abs/err	T_1 abs/err
CSF	728.90	910.02	202.07 / 260.71	222.88 / 308.30	730.00 / 0.15
GM1	3115.00	2605.50	2990.20 / 8.37	2542.50 / 2.48	3030.00 / 2.73
GM2	886.60	1033.10	818.12 / 8.37	1754.80 / 41.13	915.00 / 0.91

[b] abs-absolute value, err-relative error in %.

The multi-exponential model was able to distinguish two components occurring in the combined ROI signal. The mean relative error of the T_1 estimates was 6.27 %, and the mean relative error of the M_0 was 21.80 %. The ILT method was able to distinguish all components with a mean T_1 relative error of 1.26 %.

TABLE III. Estimated coefficients for the four-component signal.

ID	Ground-truth		Modified trust-region algorithm		ILT
	T_1	M_0	T_1 abs/err[c]	M_0 abs/err	T_1 abs/err
CSF	728.90	910.02	190.28 / 283.06	256.65 / 254.58	730.00 / 0.15
GM1	3115.00	2605.50	3002.4 / 3.75	2463.30 / 5.77	3123.30 / 0.27
GM2	886.60	1033.10	786.35 / 12.75	1739.60 / 4061	925.00 / 1.23
GM3	972.00	1112.70	1086.30 / 10.52	1189.70 / 6.47	1120.00 / 15.23

[c] abs-absolute value, err-relative error in %.

The multi-exponential model was able to distinguish three components present within the combined ROI signal. The mean relative error of the T_1 estimates was 9.00 %, and the mean relative error of the M_0 was 17.62 %. The ILT method was able to distinguish all components with a mean T_1 relative error of 4.22 %.

IV. Discussion

The task of fitting a sum of exponential functions represents a well-known ill-conditioned problem [11], meaning that multiple solutions within the desired accuracy exist. To ideally separate the exponentially decaying components, their time constants should be logarithmically spaced, and their distance should be increasing with the level of noise. The number of assumed components forms another limitation. While separating two components is generally achievable, separation of three and more components is more difficult [11]. These limitations manifest sharply in the presented results obtained using the multi-exponential model. The model was able to separate the two-component signal with an average error of 1.37 %. That was not the case with the three and four-component signals, where the average relative error of T_1 increased to 7.64 % and a single component remained undetermined (relative error of several hundred percent). The method was able to estimate the parameter T_1 more precisely (average error of 5.76 %) than the parameter M_0 (average error of 13.38 %).

More precise results were obtained using the ILT method, with the average relative error of 2.52 % in T_1 estimation. The ILT method was also able to separate all components in all signals. It should be noted that the direct ILT output is a spectrum of T_1 values, unlike in the case of the multi-exponential method. Therefore, the processing of this spectrum into the aggregate T_1 values plays a crucial role in the reliability of the component estimation and was aided with the prior knowledge of their number. The estimation of the parameter M_0 could not be compared directly. While the coefficient can be estimated, it represents only the relative proportion of a given component within the signal. Comparing the two methods using only the raw relative error numbers, the ILT method seems superior. It is capable of precise estimation, regardless of the number of components within the signal. Additionally, no prior assumption of their number is required.

V. Conclusions

Two different methods for the acquisition of the spin-lattice relaxation spectrum were compared. The ILT method has proven superior to the multi-exponential model, both in estimating the signal composition and the precision. The method requires no prior knowledge of the number of components or their distribution. The ILT method could improve the low-resolution imaging of cortical lamina by better estimating its T_1 composition.

Acknowledgment

We thank Jonáš Jamárik for his help with the English language editing.

References

[1] J. J. M. Zwanenburg, J. Hendrikse, and P. R. Luijten, "Generalized Multiple-Layer Appearance of the Cerebral Cortex with 3D FLAIR 7.0-T MR Imaging," *Radiology*, vol. 262, no. 3, pp. 995–1001, Mar. 2012, doi: 10.1148/radiol.11110812.

[2] F. De Martino *et al.*, "High-Resolution Mapping of Myeloarchitecture In Vivo: Localization of Auditory Areas in the Human Brain," *Cerebral Cortex*, vol. 25, no. 10, pp. 3394–3405, Oct. 2015, doi: 10.1093/cercor/bhu150.

[3] A. Fracasso *et al.*, "Lines of Baillarger in vivo and ex vivo: Myelin contrast across lamina at 7T MRI and histology," *NeuroImage*, vol. 133, pp. 163–175, Jun. 2016, doi: 10.1016/j.neuroimage.2016.02.072.

[4] A. Lema Dopico, S. Choi, J. Hua, X. Li, and D. M. Harrison, "Multi-layer analysis of quantitative 7 T magnetic resonance imaging in the cortex of multiple sclerosis patients reveals pathology associated with disability," *Mult Scler*, p. 1352458521994556, Feb. 2021, doi: 10.1177/1352458521994556.

[5] P.-L. Bazin, M. Weiss, J. Dinse, A. Schäfer, R. Trampel, and R. Turner, "A computational framework for ultra-high resolution cortical segmentation at 7Tesla," *Neuroimage*, vol. 93 Pt 2, pp. 201–209, Jun. 2014, doi: 10.1016/j.neuroimage.2013.03.077.

[6] R. Galbusera *et al.*, "Laminar analysis of the cerebellar cortex shows widespread damage in early MS patients: A pilot study at 7T MRI," *Multiple Sclerosis Journal - Experimental, Translational and Clinical*, vol. 6, no. 4, p. 2055217320961409, Oct. 2020, doi: 10.1177/2055217320961409.

[7] Q. X. Yang, M. B. Smith, and J. Wang, "Magnetic Susceptibility Effects in High Field MRI," in *Ultra High Field Magnetic Resonance Imaging*, P.-M. Robitaille and L. Berliner, Eds. Boston, MA: Springer US, 2006, pp. 249–284. doi: 10.1007/978-0-387-49648-1_9.

[8] D. Barazany and Y. Assaf, "Visualization of Cortical Lamination Patterns with Magnetic Resonance Imaging," *Cerebral Cortex*, vol. 22, no. 9, pp. 2016–2023, Sep. 2012, doi: 10.1093/cercor/bhr277.

[9] S. Lifshits *et al.*, "Resolution considerations in imaging of the cortical layers," *NeuroImage*, vol. 164, pp. 112–120, Jan. 2018, doi: 10.1016/j.neuroimage.2017.02.086.

[10] I. Shamir *et al.*, "A framework for cortical laminar composition analysis using low-resolution T1 MRI images," *Brain Struct Funct*, vol. 224, no. 4, pp. 1457–1467, May 2019, doi: 10.1007/s00429-019-01848-2.

[11] A. Istratov and O. Vyvenko, "Exponential analysis in physical phenomena," *Review of Scientific Instruments*, vol. 70, pp. 1233–1257, Feb. 1999, doi: 10.1063/1.1149581.

[12] J. K. Barral, E. Gudmundson, N. Stikov, M. Etezadi-Amoli, P. Stoica, and D. G. Nishimura, "A Robust Methodology for In Vivo T1 Mapping," *Magn Reson Med*, vol. 64, no. 4, pp. 1057–1067, Oct. 2010, doi: 10.1002/mrm.22497.

[13] A. R. Conn, N. I. M. Gould, and P. L. Toint, *Trust-region methods*. Philadelphia, PA: Society for Industrial and Applied Mathematics, 2000.

[14] J. Jamárik, L. Vojtíšek, V. Churová, T. Kašpárek, and D. Schwarz, "Identification of Laminar Composition in Cerebral Cortex Using Low-Resolution Magnetic Resonance Images and Trust Region Optimization Algorithm," *Diagnostics*, vol. 12, no. 1, Art. no. 1, Jan. 2022, doi: 10.3390/diagnostics12010024.

[15] E. J. Fordham, L. Venkataramanan, J. Mitchell, and A. Valori, "What are, and what are not, Inverse Laplace Transforms," pp. 1–8.

[16] C. L. Lawson and R. J. Hanson, in *Solving Least-Squares Problems*, Upper Saddle River, NJ: Prentice Hall, 1974, p. 161.